This thesis submitted in fulfillment of the requirements for the degree of Masters of Science in Mechanical Engineering

# Study of various working fluids on MEMS-based Micro-Resistojet Thruster through CFD

Pakistan Navy Engineering College,
National University of Science and Technology (NUST),
Karachi, Pakistan

M.Muzammil Ejaz
M.S (Thermal Power/ Fluid Energy)
Roll # NUST201361629MPNEC45113F

# Acknowledgement

"Read! In the name of your Lord who created - Created the human from something which clings. Read! And your Lord is Most Bountiful - He who taught (the use of) the Pen, Taught the human that which he knew not."

**[Quran, Surah Al-`ALAQ]**

Allah! Is the one who gave me strength and blessing in completing thesis?

Foremost, I would like to express my sincere gratitude to my advisor Cdr._Dr. Shafiq-Ur-Rehman and Co Advisor Dr. Noman for the continuous support of my M.S research thesis, for his patience, motivation, enthusiasm, and immense knowledge. His guidance helped me in all the time of research and writing of this thesis.

I would also like to thank our M.S Student Advisor Dr Muhammad Ali Khan and rest of my thesis committee for their encouragement and taking consistent update of thesis in form of presentation, insightful questions & comments.

I thank my Class mate specially Abdullah Aziz, Tariq, lt. Jawwad and Shiraz Ali for their moral support for the completion of this thesis.

Last but not the least; I would like to thank my parents for tire efforts for upbringing me to this place and supporting me throughout my life.

# Abstract

The development of MEOMS/ MEMS has scale down the satellites into micro, nano, pico or cube satellites. Due to their cheap manufacturing and launch cost. They are getting prevailing in space research and applications. These are now widely used in micro propulsion systems in small scale Satellites, mostly for controlling attitude. Performance of micronozzles/microthrusters in terms of thrust, Isp and viscous subsonic layer at the nozzle exit that is significant in low Reynolds number flows that adversely affects the performance of micronozzles. Therefore to optimize micronozzle/thrusters, the successful performance predictions will help in estimating the desired parameters and for the finalization of thruster configuration for its development and testing.

In this regard this thesis involves the numerical modeling (CFD), simulation and performance of proposed Micro-Resistojet thruster configuration for various working fluids will be investigated in terms of Thrust, Specific Impulse (Isp) and viscous subsonic layer at the nozzle exit. This numerical investigation will also validate our numerical CFD method with the numerical and experimental results found in various research papers.

# Table of Contents

# List of Figures

# List of Tables

# Chapter 1
# Introduction

## 1.1 Problem Statement

The flow through micro-nozzles is of great interest for researchers in the fields of automobile, aerospace, defense and biomedical engineering. The successful performance predictions will help in estimating the desired parameters and for the finalization of thruster configuration for its development and testing.

As the experimental work on microthruster already initiated in 2013 at SETC Karachi. This Thesis involves the numerical modeling (CFD), simulation and performance prediction of proposed Micro-Resistojet thruster configuration for various working fluids i.e (Nitrogen, CO2, Argon)

This Thesis involves the numerical modeling (CFD), simulation and performance prediction of proposed Micro-Resistojet thruster configuration for various working fluids. After the validation of our numerical CFD methods and results with available numerical and experimental data, a parametric study will be conducted for various working fluids the effect Thrust; Specific Impulse (Isp) and viscous subsonic layer thickness will be investigated.

## 1.2 Micro Propulsion system:

In Micro Propulsion system, Drag losses effects in satellites make it fall from their orbits and we need to reposition it as per requirement. These operations are comes as maintenance of orbit that consist of three major parts: initial orbit insertion and correction, station keeping and orbit maintenance, and end-of life maneuvers [5].

The satellites when coming to their orbits, there is small error often noted, therefore it have significant importance for satellites constellations, which is also required for a specific relative distance between them. The critically comes when accurate propulsion system able to fine tune the orbits [5]. For this importance of satellite position control and attitude control , the magnetic torquers, electrical propulsion or chemical thrusters used. For microsatellites, both mass and the size of the thrusters should be preferably small [5].

Different types of electrical propulsion and chemical systems available for micro-thruster technology are given below:

**Chemical Propulsion**

- Cold gas -------------(scaled down)
- Monopropellant ----(scaled down)
- Bipropellant
- Solid Propellant  ---(scaled down)

**Electric Propulsion**

- Resistojet ------------(scaled down)
- Hall thrusters
- Ion engines
- Pulsed Plasma Thrusters (PPT)
- Field emitted electric propulsion (FEEP)

In the fig. 1 the graph between thrust force and total mission velocity change for different chemical and electrical propulsion systems. It can be seen from the figure that chemical propulsion comes under low $\Delta v$ missions. Therefore, for a low mass budget and low $\Delta v$ missions (for example, attitude and position control) of small microsatellites and nanosatellites, chemical micropropulsion is a sound choice.

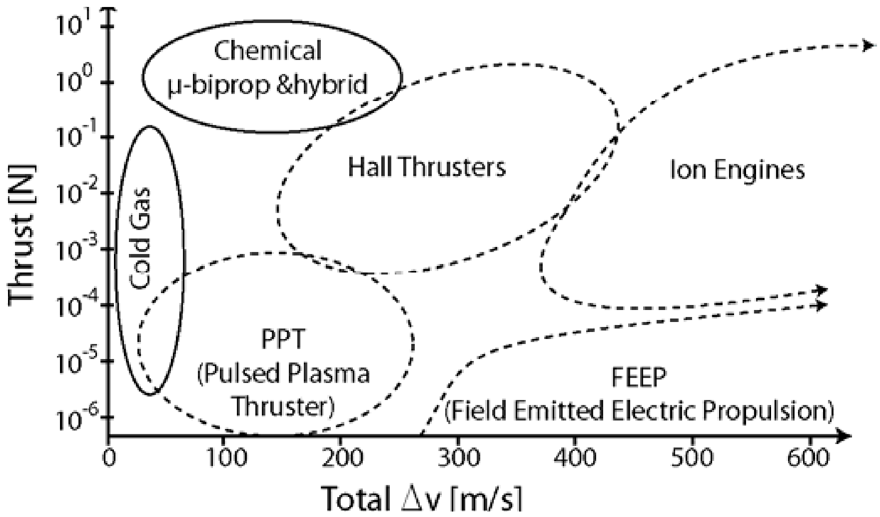


Figure No 1: Graphical presentation of available thrusters in satellites, exhibit the different microthrust systems in a thrust vs. total mission ΔV graph [5]

From the fig. 1 The Attitude control, chemical system is better and for other movement like inter planetary. Electrical Propulsion EP, FEEP, ion thrusters, Hall effect thrusters and pulsed plasma thruster (PPT), (see fig. 6) encounter high total mission (ΔV) velocity change, that produces small required forces for accurate positioning [5] .Up to date many propulsion systems used for the space exploration are chemical propulsions due to their simpler physics and higher completeness than electrical propulsions [9].

## 1.3 Resistojet:

A resistojet is a device which propels by heating propellant by electric resistively chamber and then propellant is expanded through a downstream nozzle. The schematic of a resistojet is shown in Fig. 17.

Heating of the propellant to a high temperature is an advantage as it helps to reduce the propellant load for a given mission characteristic velocity (ΔV) [27]. Among the various devices available, the resistojet is considered a good candidate. Compared to other options for obtaining high specific impulse, like ion and plasma thrusters, it is considered more promising for small ΔV missions (up to 100-200 m/s) because of the following reasons/advantages [27].

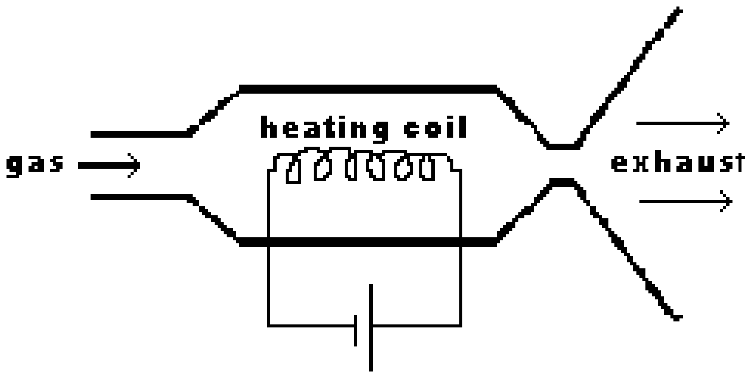


Figure 2: Schematic of a resistojet [26]

### 1.3.1 Advantages of Resistojet

- High thrust-to-power ratio
- Lowest system specific mass because of no need of power processing units
- Uncharged plume
- Usage with wide variety of propellants ($N_2$, $H_2$, Ammonia, Water, etc)
- Good performance in terms of specific impulse (100-200s)

### 1.3.2 Resistojet Applications

Resistojet is considered a good option for the attitude control of nanosatellites more promising for small ΔV missions up to 100-200 m/s [27, 28].

# 1.4 Literature Survey:

### 1.4.1 MEMS-Based Micro Resistojet Thruster Developed by TU-Delft, Netherlands

In this section, a MEMS-based micro-resistojet designed, developed and tested by the researchers at TU Delft, Netherlands is presented. The details are extracted from research papers [27,28]

This MEMS-Based micro resistojet thruster requires an integrated thin-film heater capable of heating propellant flow of 1 mg/s to 350 $^{o}$C. With nitrogen, it was demonstrated to produce a thrust between 20 μN and 1 mN. Chamber pressure values in the range of 1 - 5 bars were obtained for a propellant flow rate of 0.15 - 1.5 mg/s at cold gas mode.. Its small size (25 x 5 x 1 mm), low mass (162 mg) and low power consumption (< 3 W) are very attractive for application on cubesats. In addition, when using vaporizing liquids, like water or ammonia, as propellant, this would allow for improved performances of the thruster making it an attractive candidate for use on cubesats with mission velocity requirements of up to 50-100 m/s.

### 1.4.2 Description of Micro-Resistojet Thruster Design

The micro-resistojet thruster is fabricated in silicon MEMS technology. Therefore design should be simple that requires an integrated heating device to heat-up the propellant flow and then expended through convergent divergent nozzle to produce thrust by expansion of hot gases. (Fig. 18). To validate the device, researchers at TU Delft used cold nitrogen gas which is pressurized to hold capacity as a propellant. Then Cold nitrogen enters through inlet and then warmed by thin-film integrated heater made of aluminum. Silicon, with its high thermal conductivity of 157 W/m-K, acts as an excellent heat dissipater providing incresed temperatures at fluidic walls channel. Pressured gas at the heater channel outlet at high temperature is then expanded through the nozzle to produce thrust [27].

The schematics of this micro-resistojet configuration (as seen from the top and from the bottom) are shown in Fig. 3. In this figure, the inlet manifold, heater section and nozzle can be seen. Linear slit nozzle was chosen as the most convenient solution to be realized with the employed MEMS fabrication technique. The channels have a rectangular cross-section 50 μm wide and 150 μm deep as shown in Fig. 4. To provide a hydro-thermally fully developed flow along the channels, their length was fixed at 2 cm. The linear slit nozzle was etched along with the heater channels, having the same feature depth of 150 μm. The inlet manifold has a depth of 300 μm. Expansion ratio of the nozzle, defined as the ratio between the exit area to throat area of the nozzle, is fixed at 25. Two different nozzle throat widths were considered for the designs at TU Delft: 10 μm and 5 μm.

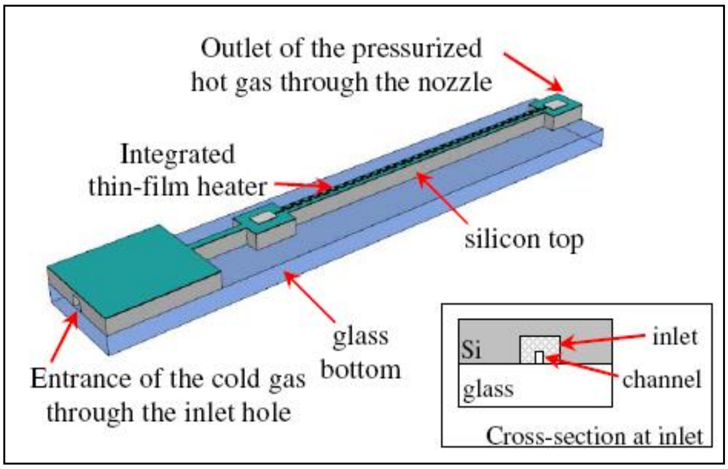


Figure 3: Schematic of the MEMS Resistojet [28]

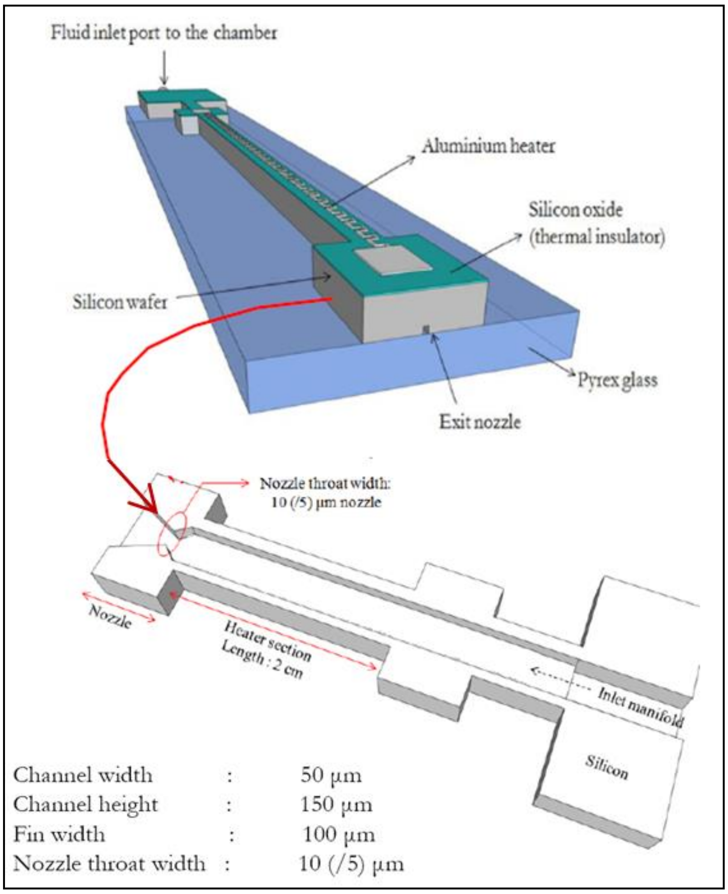


Figure 4: (Top) Schematic of MEMS micro-resistojet concept seen from top and. (bottom) seen from bottom showing inlet manifold, heater section and nozzle [27].

We have also performed CFD simulations of the viscous flow through the micro-resistojet thruster having 10 μm throat width. The details of this CFD analysis can be found in Section 4.3 of this report. The length of the inlet manifold is not given in [27,28], therefore, for numerical study we took an arbitrary length of 0.7 cm.

### 1.4.3 Experimental Set-up at TU Delft

In this section, the experimental set-up, developed by the researchers at TU Delft to test the micro-resistojet thruster, is presented. The details of this experimental set-up have been extracted from a research paper [27,28].

Figure 20 shows the schematic representation of the test setup at TU Delft [27]. The micro-resistojet device was tested inside a Heraus Vacuutherm vacuum chamber, capable of producing pressures ≤ 50 mbar. Cold nitrogen gas is stored in a bottle of 200 bar and reduced to a constant 5 bar relative pressure with a pressure regulation valve (relative pressure = absolute pressure - atmospheric pressure at sea level). The gas flow through the system is regulated by a Brooks mass flow controller of a range between 0.15 - 3 mg/s and accuracy of ±0.2% Full Scale (F.S). Regulated flow from the Flow Controller into the system is then switched ON/OFF by a Clipper Solenoid valve installed just at the vacuum inlet chamber.

1. Nitrogen gas storage tank
2. Pressure regulator
3. Mass flow controller 0.15-3 mg/s
4. Gate valve
5. Solenoid valve
6. Pressure sensor
7. Tube-to-needle adaptor
8. Needle
9. MEMS micro-resistojet thruster
10. Power sourcemeter
11. Data Acquisition (DAQ)
12. Test control PC
13. Vacuum chamber

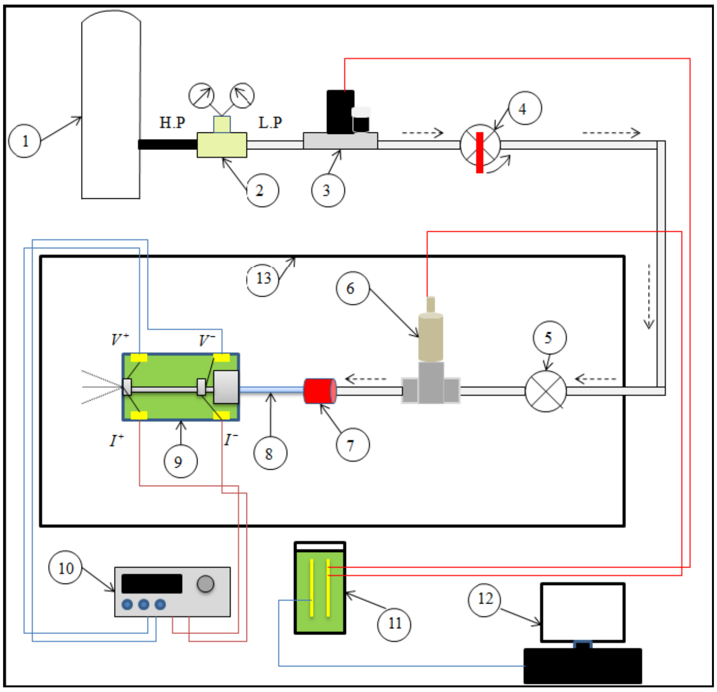


Figure 5: TU Delft measurement setup Schematic [27], consisting of vacuum chamber, MFC, pressure transducer and external source meter]

The pressure is gauged by an Omega pressure transducer, with a range of 0-6 bars absolute and an accuracy of ±0.25 % F.S. This pressure transducer gives the reading of the pressure at the device inlet. This pressure is called system pressure, $P_S$ in research papers [26, 27].The stagnation pressure at the nozzle inlet $P_C$, which is responsible for the thrust. It is calculated by taking difference of system pressure and the calculated pressure drop exhibited along the micro-channels and across the adaptor: $P_C = P_S – \Delta P$. By controlling the mass flow rate, the system pressure is set.

To perform propellant testing in devices, the heater deliver the power needed for the heating up the propellant to flow. Input current in the heater was controlled by an external power source with an input range of 0-1 A and an accuracy of ±0.05%+1.8 mA. The resistance of heater was measuring by a four-point measurement approach (TCR for aluminium = 0.0043/ºC at room temperature), the average heater temperature was calculated by using the relation given below:

$$T = T_o + \frac{1}{TCR}\left(\frac{R - R_o}{R_o}\right) \tag{1}$$

# Chapter 2
# Numerical Modelling & Simulations

## 2.1 Numerical Model Considerations for Micronozzels

A component common to any chemical-based propulsion scheme is the converging-diverging nozzle (or a *de Laval* nozzle), whose role is to produce thrust by efficiently converting the pressure/internal energy of inlet gases into kinetic energy. The pressurized propellant is first heated and then accelerates it to sub sonic flow at convergent section and then flow expended divergent section to obtain supersonic flow at nozzle throat.

The combination of high speeds and moderate-to-large length scales result in very high Reynolds numbers in traditional space propulsion applications – sufficiently large that inviscid analyses employed are as a first approximation [29]. The importance of viscous effects in supersonic flows has emerged as a result of the development of micro-scale propulsion systems. Characteristic length scales are being considered for these new propulsion systems in the order of microns to millimeters, by supersonic nozzles corresponding Reynolds No. goes within the range Re ~ $10^1$ – $10^3$ and hence viscous effects can no longer be ignored. For these scenarios the low Reynolds number, supersonic flow represents an unusual flow regime, there is the usual thermo-fluidic complexity of a supersonic flow superimposed with subsonic viscous boundary layers extending from solid surfaces in these regimes. At these low Reynolds numbers the viscous layer can occupy a sizable fraction of the divergent nozzle cross-section and, as a consequence, substantially impact the performance of the nozzle (e.g., thrust production).

Taken together, the combination of viscous/thermal /rarefaction effects on the microscale can significantly impact the flow behavior in supersonic micronozzles. Nozzles based on past macro-scale designs will exhibit performance degradations which are not predicted from traditional analyses. These degradations are especially significant for nanosat propulsion scenarios where fuel supply is inherently limited. From an engineering perspective, therefore, the accounting for these micro-scale effects is essential in the design of efficient micronozzles [29].

## 2.2 Study/Analyze Flows through Micronozzles

In addition to all the advantages and convenience of using MEMS devices, the physical phenomenon of the small scales are significantly different from the normal scale and needs to be studied and understood [29].

The physical characteristics of flow through supersonic micronozzles have been investigated with different numerical and experimental methods. Given the experimental difficulty associated with micro-scale supersonic flow interrogation, detailed flow analyses are necessarily computational in nature. As mentioned in [29], while some experimental works have also been reported in [30,31,32], these have been generally limited to bulk thrust measurements without corresponding flow field data. The lack of experimental access to supersonic flows on the microscale requires that micronozzle design be based largely on computational and/or theoretical analyses of performance [29]. In order to assess the performance of the nozzles prior to fabrication and testing, numerical simulations establish a benchmark with which the experimental work is compared [33].

Following section deals with the numerical methods to study gas flows through micronozzles.

## 2.3 Numerical Methods to Study/Analyse Micronozzle Flows

### 2.3.1 Numerical Methods for Continuum Flow Regimes

The vast majority of computational and analytical tools for studying fluid behavior are based on the Euler or Navier-Stokes equations (Computational Fluid Dynamics). An important underlying assumption of these equations is that the fluid may be treated as continuum, rather than as a collection of discrete particles, as is done in the more difficult, Boltzmann equation [34]. This allows the transport terms to be calculated using macroscopic variables, such temperature, rather than microscopic variables, such as molecular velocity distribution function, yielding an expression which is more amenable to solution, both analytically and numerically. Unfortunately, this approximation becomes inaccurate as the characteristic length of the physical domain (L) approaches the average distance travelled by a particle between collisions (the mean free path, lambda), which occurs for many MEMS-related flows. The ratio of these quantities is known as the Knudsen number (Kn=lambda/L) and is used to indicate the degree of flow rarefaction of gases encountered in MEMS devices. For supersonic nozzles the throat dimension is commonly chosen as the characteristic length scale. The Navier-Stokes equations neglect rarefaction effects and are therefore only strictly accurate for vanishingly-small Kn numbers (Kn < 0.01) [34].

An alternative version of the Knudsen number [29,36], based on the ratio of Mach number and Reynolds number, which is of particular use in investigating supersonic flows is given by

$$Kn = \sqrt{\gamma\pi/2}\,\frac{M}{Re} \qquad (2)$$

The classification of flow rarefaction regimes based on the Knudsen number is given in Fig. 6 where also the applicable governing equations for each flow regime are also indicated.

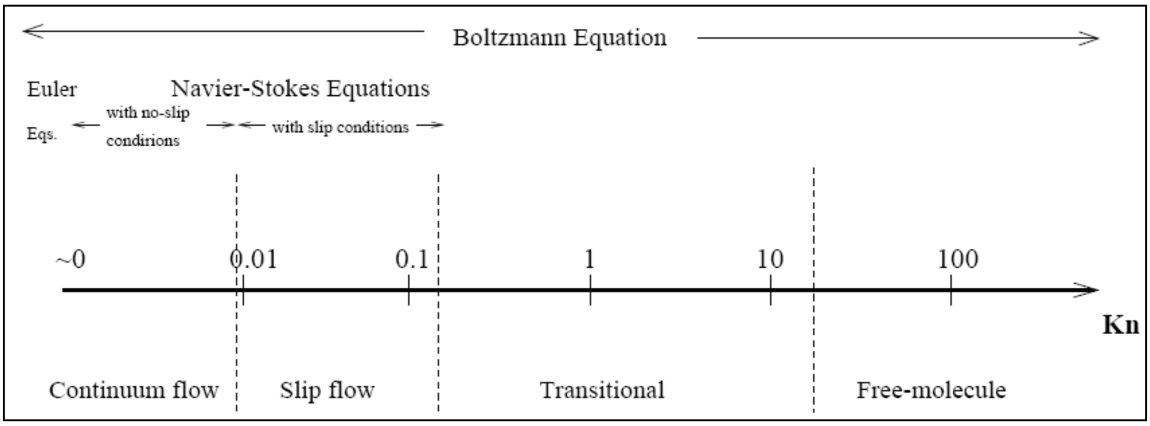


Figure 6: Flow rarefaction regimes based on Knudsen number and governing equations [35]

### 2.3.2 Numerical methods for Rarefied Flow Regime

For micronozzles at large Knudsen numbers, Kn > 0.01 at the throat, the macroscopic description of gas flows based on continuum hypothesis, such as Navier-Stokes equations (CFD techniques), breaks down and a numerical method capable of describing non-continuum, rarefied gas flows needs to be applied [29].

Particle methods, such as molecular dynamics (MD), particle-in-cell (PIC), and DSMC (Direct Simulation Monte Carlo) are attractive tools for the study of rarefied gas flows because they lack continuum assumptions [34]. These techniques model gas behavior by tracking the interaction of computational particles, each with a position, a velocity, an internal energy, etc., mimicking the discrete molecular nature of the actual flow [34]. This strategy differs considerably from that of traditional CFD, which numerically solves differential field equations formulated to describe fluid behavior in terms of macroscopic variables. [34]

DSMC is by far the most popular particle method to study rarefied gas flows in the micronozzles. It is a particle-based numerical fluid modeling technique and used for the analysis of collisional flows, that is, flows for which intermolecular collisions significantly affect fluid behavior [37]. It is called a simulation (rather than a solution) scheme because it was originally formulated to capture the important physical features of the flow, not to solve a particular set of equations [37].

## 2.4 Numerical Simulations in CFD Software Package

In Ansys Fluent the fluid flow calculation are based on the continuity, Navier Stokes momentum and the energy equation. All these equations are under a control volume setup [23].

### 2.4.1 Continuity Equation:

$$\partial\rho/\partial t + \partial\rho u/ \partial x + \partial\rho v/ \partial y + \partial\rho w/ \partial z = 0 \quad (3)$$

For stead state flow,

$$\partial\rho / \partial t = 0 \quad (4)$$

Now equation Becomes

$$\partial\rho u/ \partial x + \partial\rho v/ \partial y + \partial\rho w/ \partial z = 0 \quad (5)$$

For incompressible flow i.e. constant density, the equation 5 is reduced to

$$\partial u/ \partial x + \partial v/ \partial y + \partial w / \partial z = 0 \quad (6)$$

This approach reduces the required computational power as less inputs are fed into the computer for further processing

### 2.4.2 Momentum Equation (Navier-Stokes Equations):

Navier-Stokes equations describes the momentum balance across the fluid flow following the Newton's second law of motion. It is defined as the sum of all the forces acting in a direction is equal to the change in momentum in all directions. These forces may be either surface forces or body forces. Surface forces may include pressure and viscous forces and body forces include gravity, centrifugal and electro-magnetic forces.

$$\rho\left[\frac{\partial v_x}{\partial t}+v_x\frac{\partial v_x}{\partial x}+v_y\frac{\partial v_x}{\partial y}+v_z\frac{\partial v_x}{\partial z}\right]=\rho g\vec{\imath}-\frac{\partial P}{\partial x}+\mu\left[\frac{\partial^2 v_x}{\partial x^2}+\frac{\partial^2 v_x}{\partial y^2}+\frac{\partial^2 v_x}{\partial y^2}\right] \quad (7)$$

$$\rho\left[\frac{\partial v_y}{\partial t}+v_x\frac{\partial v_y}{\partial x}+v_y\frac{\partial v_y}{\partial y}+v_z\frac{\partial v_y}{\partial z}\right]=\rho g\vec{\jmath}-\frac{\partial P}{\partial y}+\mu\left[\frac{\partial^2 v_y}{\partial x^2}+\frac{\partial^2 v_y}{\partial y^2}+\frac{\partial^2 v_y}{\partial y^2}\right] \quad (8)$$

$$\rho\left[\frac{\partial v_z}{\partial t}+v_x\frac{\partial v_z}{\partial x}+v_y\frac{\partial v_z}{\partial y}+v_z\frac{\partial v_z}{\partial z}\right]=\rho g\vec{k}-\frac{\partial P}{\partial z}+\mu\left[\frac{\partial^2 v_z}{\partial x^2}+\frac{\partial^2 v_z}{\partial y^2}+\frac{\partial^2 v_z}{\partial y^2}\right] \quad (9)$$

Considering constant density due to incompressible flow, and constant viscosity simplifies the equation as follows which is still very difficult to solve numerically.

$$\left[v_x\frac{\partial v_x}{\partial x}+v_y\frac{\partial v_x}{\partial y}+v_z\frac{\partial v_x}{\partial z}\right]=\vartheta\left[\frac{\partial^2 v_x}{\partial x^2}+\frac{\partial^2 v_x}{\partial y^2}+\frac{\partial^2 v_x}{\partial y^2}\right]+g\vec{\imath}-\frac{\partial P}{\rho\partial x} \quad (10)$$

In CFD software, the momentum equation is often combined with continuity equation. This is due overcome the absence of pressure component in continuity equation and obtain accuracy in results. The combination results in Poisson equation as,

$$\frac{\partial}{\partial x_i}\left(\frac{\partial P}{\partial x_i}\right)=-\frac{\partial}{\partial x_i}\left(\frac{\partial(\rho U_i U_j)}{\partial x_i}\right) \quad (11)$$

For Cartesian coordinate system we shall use i, j, k = x, y, z. This equation has more suitable numerical properties and can be solved by proper iteration methods.

### 2.4.3 Energy Equation:

Kinetic energy due to the mass and velocity of the fluid, thermal energy and chemically bounded energy, are all types of energy commonly associated with fluid flow. Thus total energy is defined by,

$$h = hm + hT + hC + \Phi \quad (12)$$

Where hm is the kinetic energy, hT is the thermal energy, hC is the chemical energy and Φ is the potential energy.

Summarizing the three steady state equation we get,

Continuity equation: $$\nabla.(\rho V) = 0 \quad (13)$$

Momentum equation: $$\rho g - \nabla \mathrm{p} + \nabla.\tau_{ij} = 0 \quad (14)$$

Energy equation: $$p(\nabla.V) = \nabla.(\mathrm{k}\nabla\mathrm{T}) + \Phi \quad (15)$$

# Chapter 3
# CFD Analysis

Computational Fluid Dynamics (CFD) is a study of any system begins with the building of required geometry and mesh for modeling the domain. To model a system we discretize the domain into small volumes and equations are solved using iterative methods. Boundary conditions are then applied followed by analysis of the results.

We used CFD package for simulation including Gridgen V.15 for geometry modelling, meshing and for boundary conditions. Simulations were executed in Ansys Fluent V15 used with following steps.

## 3.1 Geometry used for Numerical Simulations

The geometry of the micro-resistojet configuration used in this numerical study has been taken from the papers [27,28] and has been simplified by modeling only the inlet manifold, heater section,. Details of this geometry can be found in [27,28] and in Fig 7, 8 &9. For numerical simulations, only half of the micro-resistojet geometry is considered. The symmetry surface (yellow surface) is shown in Fig. 8.

## 3.2 Grid and Boundary Conditions

Boundary conditions involved in numerical simulations are shown in Fig. 9 and Table2. For all simulations, the boundary condition at the device inlet consists of a fixed stagnation temperature $T_o$ (273K), along with a fixed mass flow rate (0.35 mg/s) as taking asymmetric flow taking its half (0.175 mg/s) Pressure Outlet boundary condition type is used at the micronozzle exit where a pressure of 50 Pa is defined. All the other boundaries are considered walls. Eexample of grid at the nozzle, heater and inlet manifold portion can be seen in Fig. 7, 8 & 9.

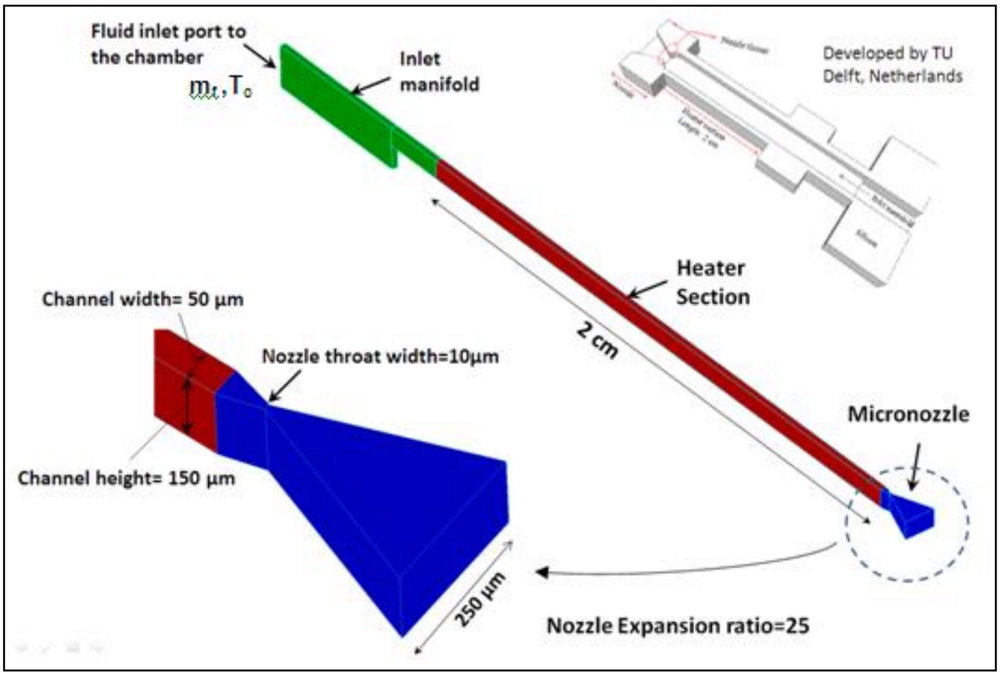


Figure 7: Simplified geometry of micro-resistojet used for numerical simulations

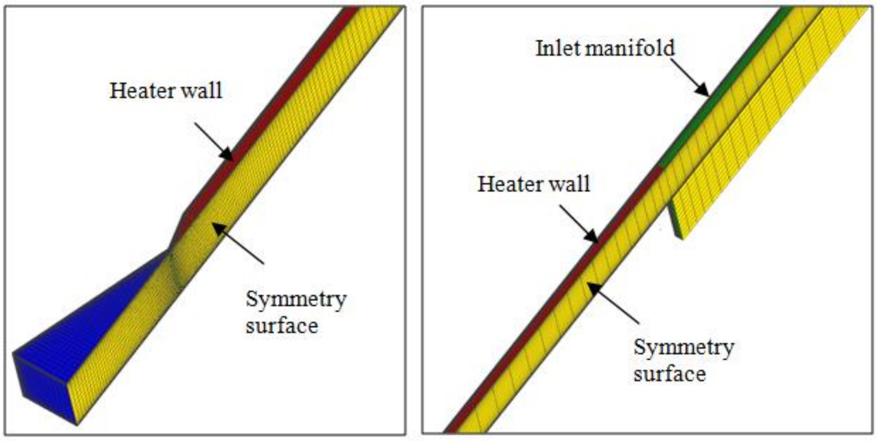


Figure 8: (Left) Nozzle region, (Right) Inlet manifold region of the micro-resistojet

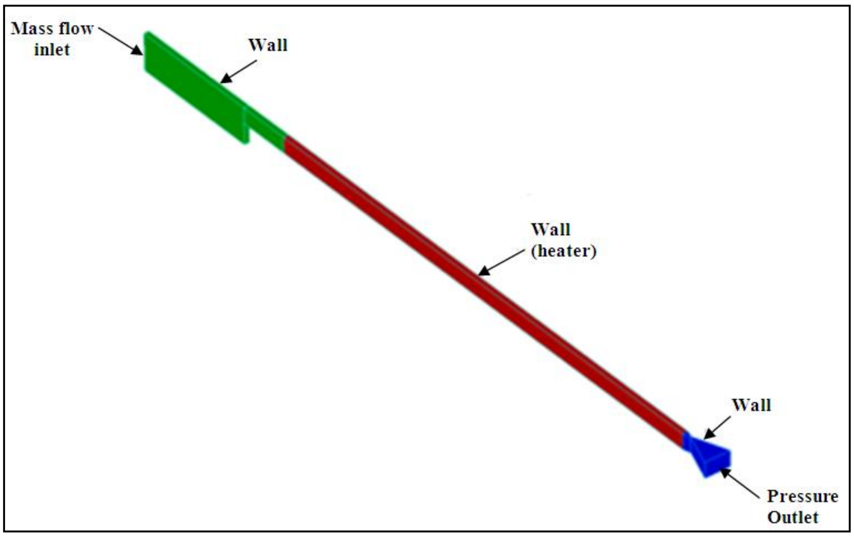


Figure 9: Boundary conditions used for numerical simulations

| Surface | Boundary Condition |
|---|---|
| Micro-resistojet device inlet | Mass flow inlet |
| Nozzle Exit | Pressure Outlet |
| Symmetry | Symmetry |
| Heater walls | Wall |
| Wall (except heater walls) | Wall |

Table 1 : Boundary conditions involved in numerical simulations

| **Simulation No.** | **Inlet Mass flow (mg/s)** | **Inlet Stagnation pressure (ºC)** | **Wall Temperature (except heater wall) (ºC)** | **Heater wall Temperature (ºC)** | **Gauge Pressure at Nozzle Exit (Pa)** |
|---|---|---|---|---|---|
| 1 | | | | 23 | |
| 2 | | | | 100 | |
| 3 | | | | 200 | |
| 4 | (0.175) | 23 | 23 | 300 | 50 |
| 6 | | | | 400 | |
| 7 | | | | 500 | |

Table 2 : CFD simulation plan for the current problem

## 3.3 Fluid Properties

In ANSYS FLUENT®, the properties of the working fluid (Nitrogen, $Co_2$ and Argon) are defined as follows:

| Property | Units | Method | Value |
|---|---|---|---|
| Density | $kg/m^3$ | Ideal Gas | Variable |
| $C_p$ (Specific Heat) | J/kg-K | Piecewise-Polynomial | Variable |
| Thermal Conductivity | W/m-K | Kinetic Theory | Variable |
| Viscosity | kg/m-s | Sutherland Law | Variable |
| Mol. wt | Kg/kmol | Constant | 28.0134 |

Table 3: Properties of Nitrogen used for computations

| Property | Units | Method | Value |
|---|---|---|---|
| Density | $kg/m^3$ | Ideal Gas | Variable |
| $C_p$ (Specific Heat) | J/kg-K | Piecewise-Polynomial | Variable |
| Thermal Conductivity | W/m-K | Kinetic Theory | Variable |
| Viscosity | kg/m-s | Sutherland Law | Variable |
| Mol. wt | Kg/kmol | Constant | 44.00995 |

Table 4: Properties of $CO_2$ used for computations

| Property | Units | Method | Value |
|---|---|---|---|
| Density | $kg/m^3$ | Ideal Gas | Variable |
| $C_p$ (Specific Heat) | J/kg-K | Piecewise-Polynomial | 520.3226 |
| Thermal Conductivity | W/m-K | Kinetic Theory | Variable |
| Viscosity | kg/m-s | Sutherland Law | Variable |
| Mol. wt | Kg/kmol | Constant | 39.948 |

Table 5: Properties of Argon used for computations

## 3.4 Numerical Approach

Micro channel flow experienced very low Reynolds No, where Knudsen No. (Kn<.01). For our current problem of steady laminar flow, The preferable CFD Model in commercial CFD software ANSYS-FLUENT®.is pressure-based solver using Laminar Stead Flow and default scheme SIMPLE or SIMPLEC. As defined in Fluent 6.3 User Guide [35]. The pressure-based solver allows to solve your flow problem in either a segregated or coupled manner. ANSYS-FLUENT®. Provides the option to choose among five pressure-velocity coupling algorithms: SIMPLE, SIMPLEC, PISO, Coupled, and (for unsteady flows using the non-iterative time advancement scheme (NITA) Fractional Step (FSM). These schemes are referred to as the pressure-based segregated algorithm. Steady-state calculations will generally use SIMPLE or SIMPLEC, while PISO is recommended for transient calculations. PISO may also be useful for steady-state and transient calculations on highly skewed meshes. In FLUENT, using the Coupled algorithm enables full pressure-velocity coupling, hence it is referred to as the pressure-based coupled algorithm. All the aforementioned schemes, except the "coupled" scheme, are based on the predictor-corrector approach. Note that SIMPLE, SIMPLEC, PISO, and Fractional Step use the pressure-based segregated algorithm, while Coupled uses the pressure-based coupled solver SIMPLE is the default.

### 3.4.1 Choosing the Pressure-Velocity Coupling SIMPLE Method:

Base on Reynold no < 2000, viscous laminar model is used in ASNYS FLUENT and it is already discussed earlier in Chapter 2 that microchannel experience low Reynold number. Therefore for our case of simple geometry of micro channel, laminar flows with no additional models activated is used and the pressure-velocity coupling default scheme in ASNYS FLUENT, SIMPLE method is used with second-order discretization. The working fluid used is $N_2$, $CO_2$ and Argon. The supersonic initial gauge pressure was set at 100 Pa then it was set to 50 Pa to compare results with reference [28, 29].

| **Under-Relation Factors** | **Values** |
|---|---|
| Pressure | 0.5 |
| Momentum | 0.5 |
| Density | 0.5 |
| Body Forces | 1 |
| Energy | 0.5 |

Table 6: Under-relaxation factors used for numerical simulation

The under-relaxation factors used for second order CFD simulations are given in Table 6. Under relaxation used in CFD software package FLUNET due to the non-linearity of equation. It is used to stabilize the convergence by controlling the change of $\phi$ by under relaxation variables which reduced it by each iteration. So the computed change is $\Delta\ \phi$ and under-relaxation factor $\alpha$ in Eq. no 16. As described in the Fluent User guide Ref [35]

$$\phi = \phi_{\text{old}} + \alpha \Delta \phi \qquad (16)$$

### 3.4.2 Measure of Convergence

CFD simulations have been performed on the micro-resistojet geometry for different heater wall temperatures according to the plan given in Table 2. For all the simulations, mass flow rate ($m_f$) of 0.175 mg/s (due to Symmetry) and stagnation temperature of 23 $^oC$ have been used at the micro-resistojet inlet. Temperature of walls (except heat walls) is maintained at 23 $^oC$ and pressure at nozzle exit at 50 Pa for each simulation. When the residuals dropped to about $10^{-10}$, they stopped changing and also the momentum thrust values were found to be not changing with further iterations. Hence, the solution was considered as being converged.

## 3.5 Grid Independence Study

To investigate the sensitivity of the grid on the numerical results, simulations have been performed using three 3-D structured grids M1, M2 and M3, having 797808, 13334000 and 2478408 quadrilateral cells respectively with Slip enable condition and without as default without slip condition that available in Fluent V15 laminar scheme. These grids have been generated using commercial grid generation software Gridgen® V15. The numerically predicted percentage (%) of exit area of nozzle is covered by layer of viscous subsonic, which is calculated by dividing subsonic region area by total nozzle exit area that shown in Table 7. Flow Rate flux is difference of mass flow rate at inlet and exit of microthrusters that shows level of convergence. (**M1= 797808 cells, M2=1334000 cells, M3=2478408 cells)**

| Parameter | Unit | Mesh Sizes | | | | | |
|---|---|---|---|---|---|---|---|
| | | Without Slip Conditions | | | With Slip Conditions | | |
| | | 0.7M | 1.3M | 2.4M | 0.7M | 1.3M | 2.4M |
| Subsonic Area | m2 | 4.03E-09 | 4.82E-09 | 4.81E-09 | 2.05E-09 | 3.80E-09 | 3.80E-09 |
| Total Area | m2 | 1.88E-08 | 1.88E-08 | 1.88E-08 | 1.88E-08 | 1.88E-08 | 1.88E-08 |
| Area % | % | 21.508 | 25.68 | 25.64 | 10.93333 | 20.29 | 20.29 |
| Flow Rate Flux | | 1.00E-10 | 5.99E-11 | 1.31E-08 | 6.46E-06 | 1.67E-09 | 4.26E-08 |

Table 7: Grid Independence study: CFD results obtained using grids of different sizes (Heater wall temp =23 $^oC$)

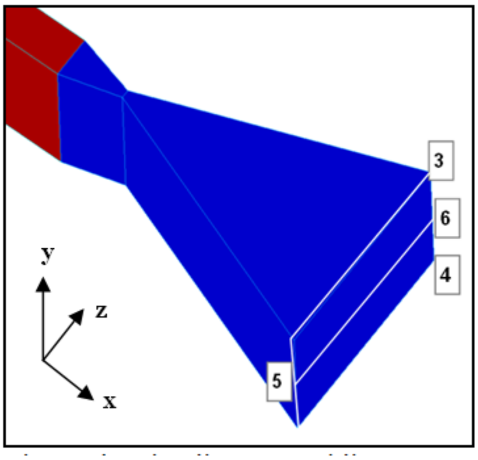


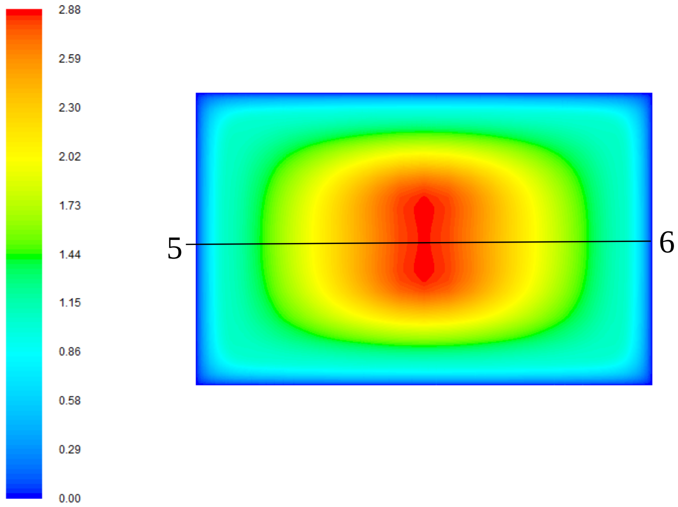


Figure 10: Line 3-4 and line 5-6 at nozzle exit

Figure 11: Contours of Mach No Line 3-4 and line 5-6 at nozzle exit

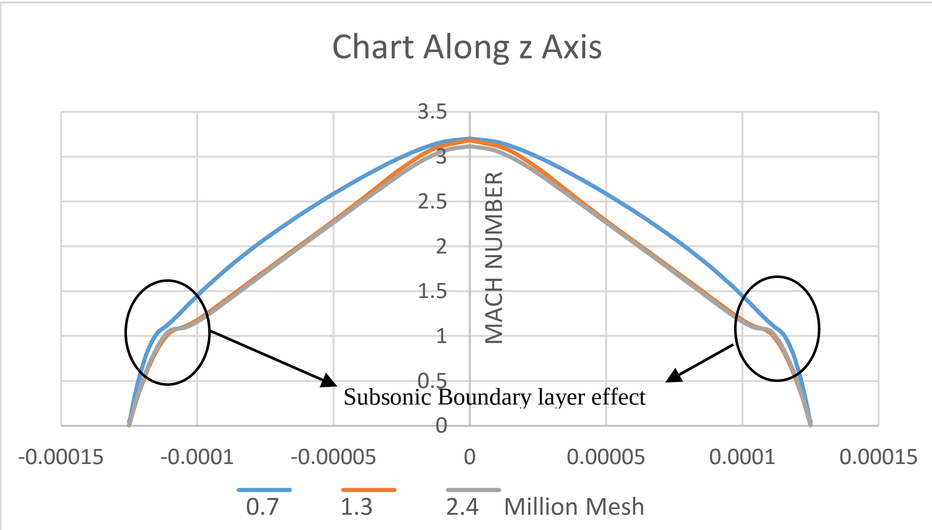


Figure 12: Centerline Mach number at nozzle exit cross-section (line 5-6)

### 3.5.1 Grid Selection:

The Mach number variation is determined along line 5-6 (shown in Fig. 11) at nozzle exit. The centerline variations of Mach number at nozzle exit along the line 5-6 for different grids are shown in Fig. 12 respectively. In the Fig. 12 the change in pattern after 1 Mach no is due to sub sonic boundary layer, that is also a performance parameter for nozzle efficiency So as we can see that 0.7 Million mesh do not cover those layer finely, whereas 1.3 and 2.4 Million mesh follow same route and also it can be seen from these figures and Table 7 that there is no significant difference in numerical results obtained by 1.3 Million and 2.4 Million mesh grids. Therefore we selected M2 grid having 13334000 quadrilateral cells and all numerical results presented in this report were obtained using this grid.

# Chapter 4

# Validation & Results Discussion

## 4.1 Validation of Numerical Method

To verify the Numerical method based on ANSYS Fluent Laminar flow model with no option activated i.e. with slip condition. We need to validate Reynold No for viscous Laminar Model and Knudsen No for microchannel continuum flow regime as per described in Chapter 2 and below Table No. 8.

| **Flow Model Limitation** | **Parameter range** |
|---|---|
| Laminar Flows | Reynold No < 2000 |
| Continuum Flow | Knudsen No > 0.01 |

Table 8: Laminar Flow model validation range

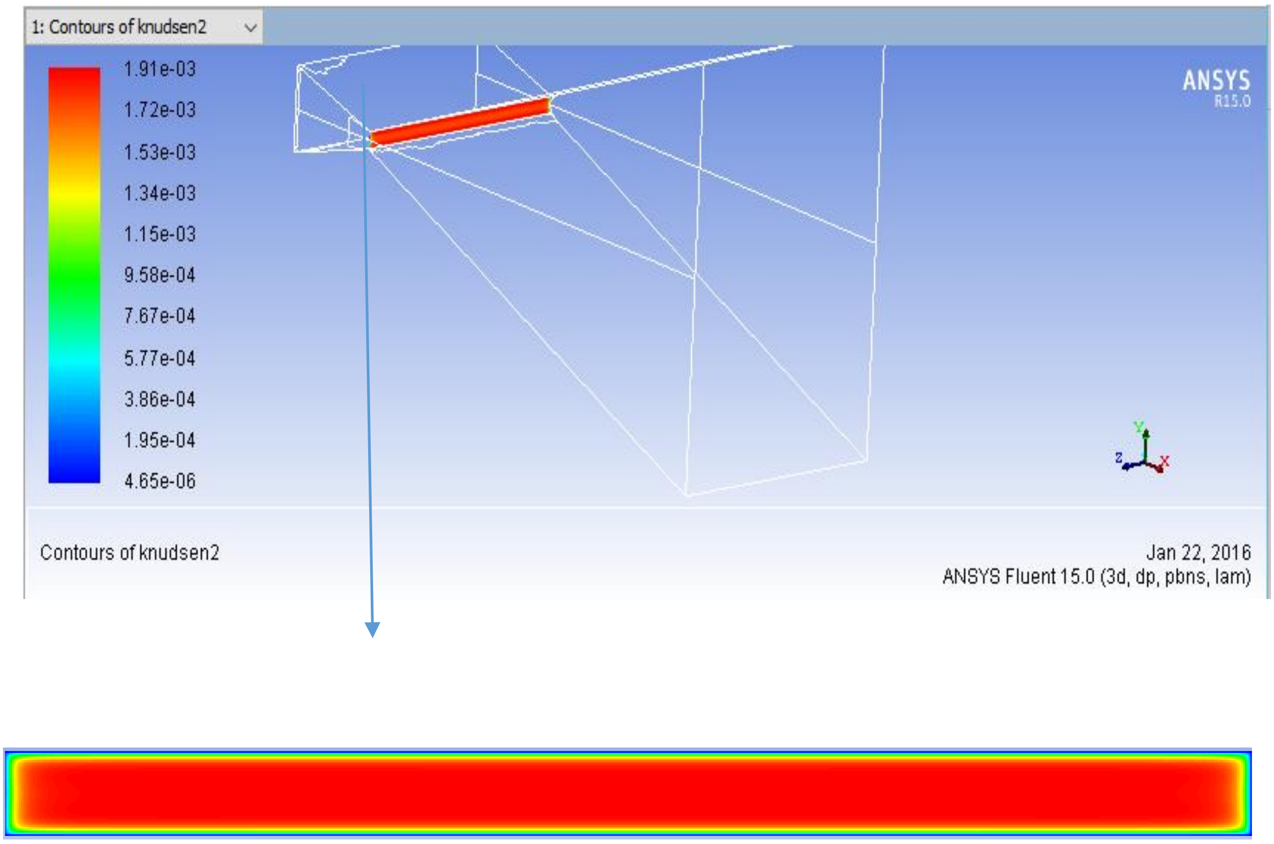


Figure 13: Contours of Knudsen No. at Nozzle Throat

### 4.1.1 Laminar Flow Validation:

Reynold Number is ratio of inertial forces to viscous forces which is used to predict the flow pattern (i.e. Laminar or turbulent). Therefore from the below Eq. 17 maximum Reynold No. is calculated at nozzle throat to check the laminar flow for $N_2$, $CO_2$, and Argon gas at different heater temperature as examined in Stnaley P. Grisnick research paper [36] . CFD Laminar flow pattern for our micro thruster also illustrated in Fig 17, 18 & 19.

$$\mathrm{Re} = \frac{\rho \mathbf{v} D_H}{\mu} = \frac{\mathbf{v} D_H}{\nu} = \frac{\mathbf{Q} D_H}{\nu A} \qquad (17)$$

| S. No | Heater Temperature ( C) | Max Reynold No. At Nozzle Throat | | |
|---|---|---|---|---|
| | | $NO_2$ | $CO_2$ | Argon |
| 1 | 23 | 739 | 885 | 611 |
| 2 | 100 | 617 | 707 | 510 |
| 3 | 200 | 522 | 568 | 419 |
| 4 | 300 | 455 | 483 | 362 |
| 5 | 400 | 406 | 422 | 321 |
| 6 | 500 | 371 | 380 | 286 |

Table 9: Reynolds number for $N_2$, $CO_2$ & Argon at different heater temperature

As shown in Table 9, all values are Re < 2000 which means that our current is valid for selected laminar flow model

### 4.1.2 Continuum Flow Regimes Validation for Microchannel

In order to verify continuum approach for our current micro channel flows problem, we need to calculate Knudsen number from CFD simulation data at the throat region for $N_2$, $CO_2$ and Argon gas at different heater temperatures. Then these values need to compare with allowable range of continuum flow regimes as describe Boltzmann Eq chart. Fig No.6 section 2.3.1.

| S. No | Heater Temperature ( C) | Max Knudsen No. At Nozzle Throat | | |
|---|---|---|---|---|
| | | $NO_2$ | $CO_2$ | Argon |
| 1 | 23 | 0.00191 | 0.001544 | 0.004019 |
| 2 | 100 | 0.002222 | 0.001905 | 0.004202 |
| 3 | 200 | 0.002363 | 0.002342 | 0.005325 |
| 4 | 300 | 0.002995 | 0.002708 | 0.006393 |
| 5 | 400 | 0.003333 | 0.003034 | 0.007399 |
| 6 | 500 | 0.003613 | 0.003362 | 0.009086 |

Table 10: Maximum values of Knudsen number occurring at nozzle throat plane

For a range of heater temperatures

The maximum values of Knudsen number are given in Table 10 . It can be seen from the Table that the maximum values of Knudsen number are less than 0.01 which means that the continuum approach is valid to solve the current problem.

## 4.2 Validation of Numerical Model from Experimental Reference

In order to validate our CFD results, we compared them with experimental results of TU Delft given in research papers [28, 29].

### 4.2.1 TU Delft Experimental Measurement Setup [28,29]

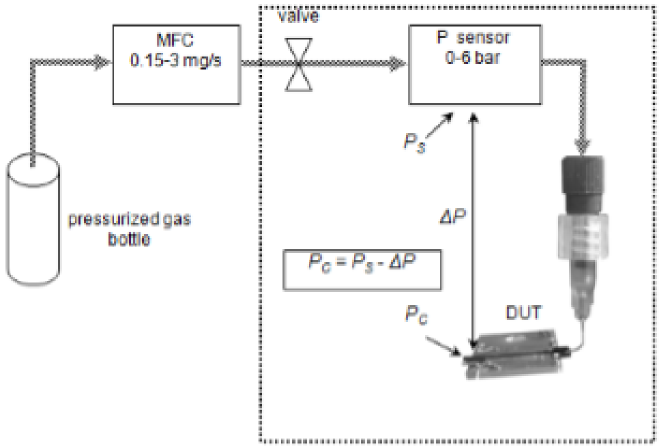


Figure 14: TU DELF Experimental setup

In TU Delft T.V Methew Research paper [28, 29], Testing setup consist of parts shown in above schematic figure No 14. Which is also defined in section 1.4.3. The pressure is gauged by an Omega pressure transducer, with a range of 0-6 bars absolute and an accuracy of ±0.25 % F.S. This pressure transducer gives the reading of the pressure at the device inlet. This pressure is called system pressure, $P_S$ in research papers [26, 27].The stagnation pressure at the nozzle inlet $P_C$, which is responsible for the thrust. It is calculated by taking difference of system pressure and the calculated pressure drop exhibited along the micro-channels and across the adaptor: $P_C = P_S – \Delta P$. By controlling the mass flow rate, the system pressure is set.

### 4.2.2 Comparison of Results from TU Delft Research paper [28]

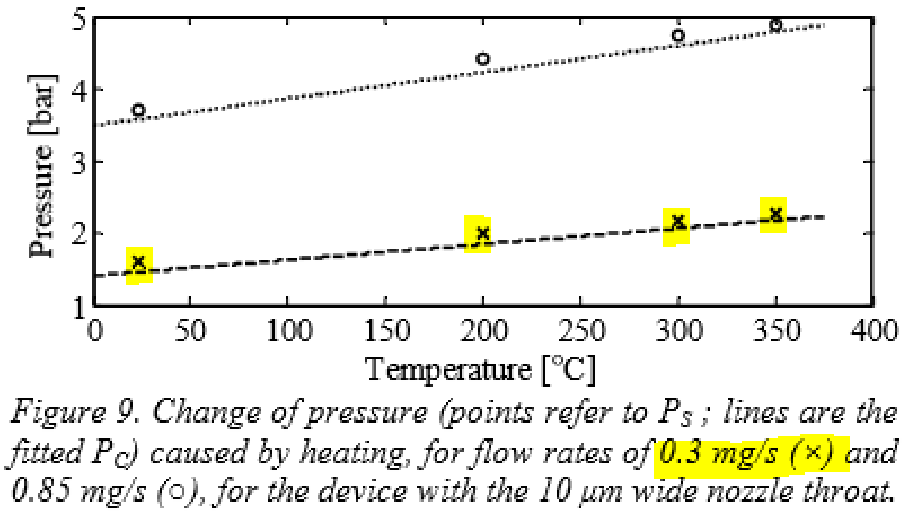


Figure 15: Pressure Vs Temperature graph form TU Delft research paper [28]

| Heater Temperature | Experimental (TU Delft Research Paper [28] | Nozzle Inlet Pressure, | Our CFD Results | % difference between numerical and experimental results |
|---|---|---|---|---|
| | System Pressure, $P_S$ | $P_{C(exp)} = P_S$ - ΔP | Nozzle Inlet pressure, $P_C$ | ( $P_{cexp}$-$P_C$) Pcexp/*100 |
| (°C) | (bar) | (bar) | (bar) | (%) |
| 23.000 | 1.605 | 1.444347 | 1.1162 | 22.7 |
| 100.000 | 1.707977 | 1.5371793 | 1.2778 | 16.8 |
| 200.000 | 2.014 | 1.8126 | 1.477 | 18.5 |
| 300.000 | 2.184 | 1.965582 | 1.644 | 16.3 |
| 400.000 | | | 1.814 | |
| 500.000 | | | 1.954 | |

Table 11: Nozzle Inlet Pressure Vs Heater Temperature Comparisons of CFD results with References [28]

### 4.2.3 Comparison of Results from TU Delft Research Journal [29]

| Heater temperature $T_h$ [°C] | System pressure, $p_{sys}$ [bar] | | | | |
|---|---|---|---|---|---|
| | Chip #19 (m=0.35 mg/s) | Chip #19 (m=1 mg/s) | Chip #11 (m=0.3 mg/s) | Chip #14 (m=0.35 mg/s) | Chip #17 (m=0.35 mg/s) |
| 23 | 1.64 | 3.86 | | 2.03 | |
| 50 | | | 3.26 | | |
| 100 | 1.88 | | 3.50 | 2.27 | 3.50 |
| 150 | | | 3.61 | | 3.68 |
| 200 | 2.05* | 4.42 | 3.70 | 2.56 | 3.77 |
| 250 | | | | | 3.82 |
| 300 | 2.19 | 4.76 | | | 3.92 |
| 350 | 2.29 | 4.92 | | | |

**- The reported value is the average of two system pressures recorded at the same mass flow rate and heater temperature during two different hot gas test campaign performed in different dates.*

Table 12: Pressure Vs Temperature graph form TU Delft research paper [29]

| Heater Temperature | Experimental (TU Delft Research Journal [29] | Nozzle Inlet Pressure, | Our CFD Results | % difference between numerical and experimental results |
|---|---|---|---|---|
| | System Pressure, $P_S$ | $P_{Cexp}=P_S - \Delta P$ | Nozzle Inlet pressure, $P_C$ | $(P_{cexp}-P_C)$ Pcexp/*100 |
| (°C) | (bar) | (bar) | (bar) | (%) |
| 23.000 | 1.640 | 1.476 | 1.1162 | 24.3 |
| 100.000 | 1.880 | 1.692 | 1.2778 | 24.4 |
| 200.000 | 2.050 | 1.845 | 1.477 | 19.9 |
| 300.000 | 2.190 | 1.971 | 1.644 | 16.5 |
| 400.000 | | | 1.814 | |
| 500.000 | | | 1.954 | |

Table 13: Nozzle Inlet Pressure Vs Heater Temperature Comparisons of CFD results with References [29]

Table 11 & 13 are the comparison tables for Reference 1 & 2 respectively. Both tables shows the comparison of results for nozzle inlet pressure, $P_C$ for different heater temperatures. The 2nd column in the table contains system pressure, $P_S$ values obtained during experiments conducted by researchers at TU Delft for different heater temperature. In the experiments [28, 29], the nozzle inlet stagnation pressure $P_C$ is calculated by taking difference of measured system pressure and the calculated pressure drop: $P_C = P_S – \Delta P$. $\Delta P$ is the pressure drop exist in device itself and adapter. The actual experimental values of $P_C$ are not given in the paper [27]. Therefore, in order to find the experimental values of $P_C$, we need to know the value of $\Delta P$.

From the paper [28], we found that the $\Delta P$ in their experimental set-up is around 10% of $P_S$. Therefore we subtracted $\Delta P$ (10% of $P_S$) from each value of $P_S$ given in the third column of the table and presented the resulting $P_C$ values in the 3rd column of the table.

From figure 16 we see that the system pressure is increasing in a linear fashion with the heater temperature for a given propellant mass flow rate for all the micro-thrusters. From the calculated heater temperature values plotted along the x-axis,

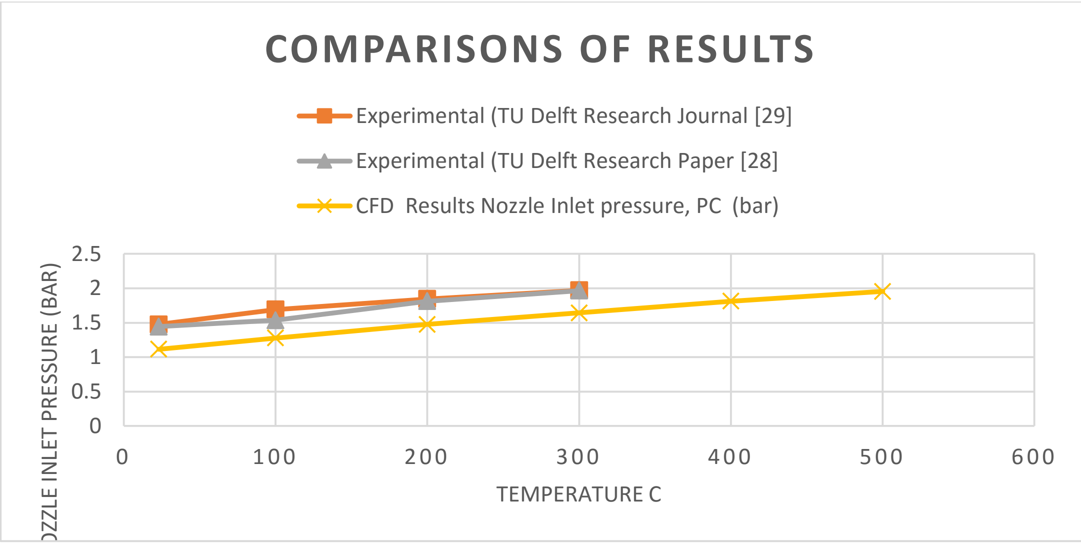


Figure 16: Nozzle Inlet Pressure Vs Heater Temperature Comparisons of CFD results with References [28], [29]

Figure 16 shows the variation of $P_C$ with heater temperature. It can be seen that CFD predicts lower $P_C$ values than those obtained by experiments. Since in the research journal [29] reveals that the leakage from feed system was to be found significant in the order of 20 ~30 % i.e. the derived chamber pressure was found to be higher than ideal for all cases, even after taking account the leakage effects. Also the discrepancies in pressure values may be due to the unknown length of the inlet manifold that was arbitrarily taken as 0.7 cm for CFD simulations

## 4.3 Performance Prediction of Nozzle:

Thrust is a force which is generated by the reaction of accelerating a mass of gas, as explained by Newton's third law of motion. A gas or working fluid is accelerated to the rear and the nozzle are accelerated in the opposite direction.

From “Newton's second law of motion”,

$$F = (m \, . V2) - (m \, . V1) \,/\, (t2 - t1) \qquad (18)$$

Where **(F)** is force, **(m)** is mass and **(V)** is Velocity across two times **(t1)** and **(t2)**

By keeping the mass constant and changing velocity with time then force is simply mass time acceleration

$$F = m \, . a \qquad (19)$$

The important parameter is **m** which is mass flow rate, equal to **(r)** density times **(V)** velocity times **(A)** the area Aerodynamicists denote this parameter as **m dot** shown with little dot above

$$\dot{m} = r \, . V \, A \qquad (20)$$

Mathematicians, scientists, and engineers used the "dot" as a symbol for "d/dt", which is equal to variable changes with a change in time. Now we can write this equation to

$$F = d(mv)/dt \qquad (21)$$

*S*o the mass flow rate is "m dot". The exit of device will denote as “e” and free stream from station "a".

$$F = (\dot{m} \cdot V)e - (\dot{m} \cdot V)a \qquad (22)$$

This **(F)** is just moment force but one additional effects of differential pressure must be accounted if the pressure at exit is different from the stream. This additional effect is the difference of pressure in the flow is an additional change in momentum. This extra force term equal to the exit area **Ae** times the pressure at exit and difference the free stream pressure across the exit area. Then the total thrust equation is becomes:

$$Ft = \left(\dot{m} \cdot V\right)e - \left(\dot{m} \cdot V\right)a + (Pe - Pa) \cdot Ae \qquad (23)$$

The gross thrust of the engine is denoted on first term on the right hand side of this equation, while the ram drag is second term. It is subtracted from the gross thrust so it is a drag term.

$$F = \left(\dot{m}\right)eng \, . (Ve - Va) \qquad (24)$$

Therefore the total thrust of at the exit of Nozzle is simplified into below equation.

$$Ft = \left(\dot{m} \,.\, V\right)e + (Pe - Pa) \,.\, Ae \qquad (25)$$

$$\boldsymbol{Ft = \dot{m} \,.\, Ve + Pe.\, Ae - Pa.\, Ae} \qquad (\mathbf{26})$$

To check useful rocket performance, there is a parameter **Isp** called as specific impulse, which completely removed dependence of the mass flow in analysis. It is the **impulse** delivered per unit of propellant consumed, and is dimensionally equivalent to the thrust generated per unit propellant flow rate.

$$\boldsymbol{Isp = Ft / (\dot{m} \cdot g_{\circ})} \qquad (\mathbf{27})$$

### 4.3.1 CFD Results of Nozzle Performance Parameters for $N_2$, $CO_2$ & Argon:

Simulations results are shown in below Table 14, 15 & 16 for $N_2$ $CO_2$ and Argon respectively. Total Thrust, Specific Impulse are calculated by Eq. 26 and Eq. 27 respectively and Sub Sonic area are calculated directly by calculating sub sonic flow area at nozzle exit area along with heater temperature variation. Flow rate flux are also shown to represent the degree of convergence. i.e < exp-10

| Properties | Unit | CFD Results for Nitrogen gas ($N_2$) | | | | | |
|---|---|---|---|---|---|---|---|
| Heater Temperature | °C | 23 | 100 | 200 | 300 | 400 | 500 |
| mdot *Ve | mN | 0.095 | 0.103 | 0.113 | 0.121 | 0.128 | 0.135 |
| PeAe | mN | 0.018 | 0.021 | 0.022 | 0.026 | 0.028 | 0.033 |
| PaAe | mN | 0.001 | 0.001 | 0.001 | 0.001 | 0.001 | 0.001 |
| Total Thrust | mN | 0.223 | 0.246 | 0.267 | 0.292 | 0.311 | 0.335 |
| Specific Impulse (Isp) | Sec | 65.1 | 71.5 | 77.9 | 85.0 | 90.6 | 97.6 |
| Subsonic Area | m2 | 4.52E-09 | 4.81E-09 | 5.40E-09 | 5.50E-09 | 5.73E-09 | 5.57E-09 |
| Total Area | m2 | 1.88E-08 | 1.88E-08 | 1.88E-08 | 1.88E-08 | 1.88E-08 | 1.88E-08 |
| Percent SubSonic Area | % | 24.12 | 25.67 | 28.77 | 29.34 | 30.54 | 29.72 |
| Flow Rate Flux | kg/s | 5.17E-10 | 5.53E-11 | -1.26E-12 | 5.90E-11 | 2.53E-12 | -2.25E-12 |

Table 14: CFD Nozzle Performance parameter for $N_2$

| Properties | Unit | CFD Results for Carbon dioxide gas ($CO_2$) | | | | | |
|---|---|---|---|---|---|---|---|
| Heater Temperature | °C | 23 | 100 | 200 | 300 | 400 | 500 |
| mdot *Ve | mN | 0.081 | 0.087 | 0.095 | 0.101 | 0.105 | 0.110 |
| PeAe | mN | 0.013 | 0.015 | 0.020 | 0.023 | 0.029 | 0.031 |
| PaAe | mN | 0.001 | 0.001 | 0.001 | 0.001 | 0.001 | 0.001 |
| Total Thrust | mN | 0.186 | 0.203 | 0.226 | 0.246 | 0.264 | 0.280 |
| Specific Impulse (Isp) | Sec | 54.2 | 59.2 | 65.9 | 71.7 | 77.0 | 81.6 |
| Subsonic Area | m2 | 4.42E-09 | 4.62E-09 | 4.70E-09 | 4.83E-09 | 4.86E-09 | 5.02E-09 |
| Total Area | m2 | 1.88E-08 | 1.88E-08 | 1.88E-08 | 1.88E-08 | 1.88E-08 | 1.88E-08 |
| Percent SubSonic Area | % | 23.59 | 24.63 | 25.08 | 25.76 | 25.91 | 26.78 |
| Flow Rate Flux | kg/s | -1.55E-12 | -1.99E-11 | 9.38E-12 | 4.51E-10 | 4.55E-10 | -1.76E-11 |

Table 15: CFD Nozzle Performance parameter for $CO_2$

| Properties | Unit | CFD Results for Argon gas (Ar) | | | | | |
|---|---|---|---|---|---|---|---|
| Heater Temperature | °C | 23 | 100 | 200 | 300 | 400 | 500 |
| mdot *Ve | mN | 0.074 | 0.081 | 0.088 | 0.095 | 0.100 | 0.104 |
| PeAe | mN | 0.016 | 0.014 | 0.018 | 0.021 | 0.024 | 0.031 |
| PaAe | mN | 0.001 | 0.001 | 0.001 | 0.001 | 0.001 | 0.001 |
| Total Thrust | mN | 0.178 | 0.189 | 0.211 | 0.230 | 0.248 | 0.268 |
| Specific Impulse (Isp) | Sec | 51.8 | 55.0 | 61.3 | 66.9 | 72.1 | 78.2 |
| Subsonic Area | m2 | 5.29E-09 | 6.21E-09 | 6.36E-09 | 6.50E-09 | 6.58E-09 | 6.64E-09 |
| Total Area | m2 | 1.88E-08 | 1.88E-08 | 1.88E-08 | 1.88E-08 | 1.88E-08 | 1.88E-08 |
| Percent SubSonic Area | % | 28.22 | 33.13 | 33.91 | 34.65 | 35.11 | 35.39 |
| Flow Rate Flux | kg/s | -1.35E-10 | 1.32E-10 | 3.85E-09 | 7.87E-11 | 8.67E-10 | -9.95E-11 |

Table 16: CFD Nozzle Performance parameter for Argon

### 4.3.2 Total Thrust of Nozzle:

From The eq (26), we have calculated total thrust and compare results across $N_2$, $CO_2$ and Argon. In Table 17 results values are represented and its graphical form in Fig. 21.

| Total Thrust (mN) | | | |
|---|---|---|---|
| **Temperature ( C)** | **Nitrogen** | **Co2** | **Argon** |
| **23** | 0.22336518 | 0.18252 | 0.17771492 |
| **100** | 0.24564362 | 0.20179 | 0.1887286 |
| **200** | 0.26739274 | 0.22486 | 0.21050586 |
| **300** | 0.29184824 | 0.24885 | 0.22982 |
| **400** | 0.3111785 | 0.26324 | 0.24772282 |
| **500** | 0.33526768 | 0.28286 | 0.26836302 |

Table 17: Total Thrust of $N_2$, $CO_2$ and Argon across heater temperature

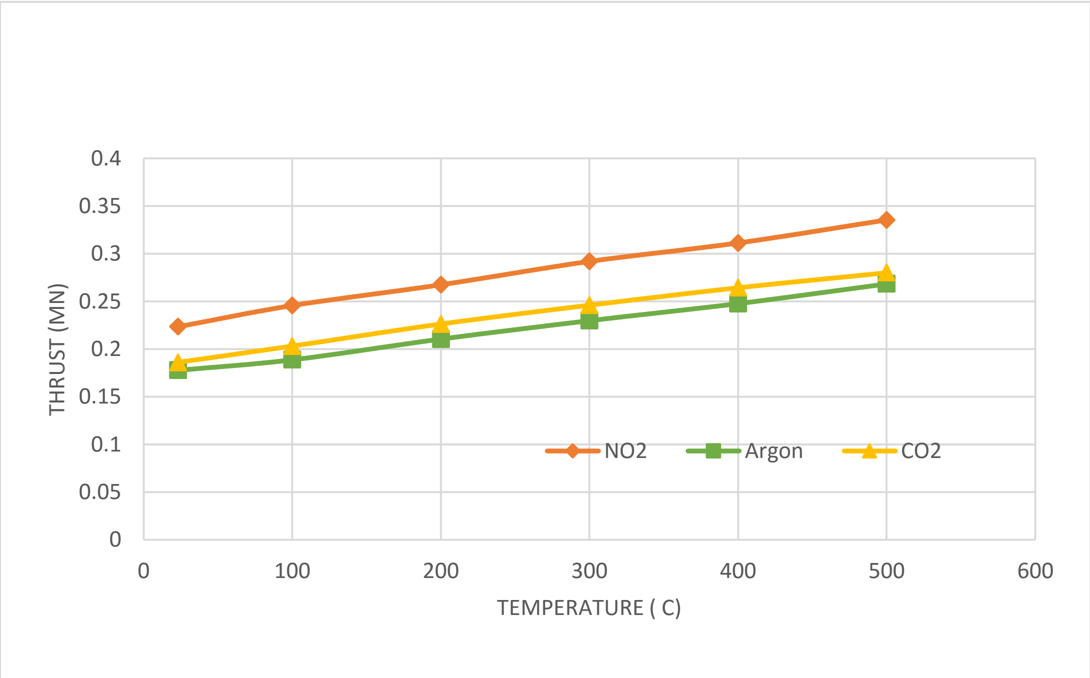


Figure 17: Total Thrust of $N_2$, $CO_2$ and Argon across heater temperature

When no heating is provided to the propellant (or when the heater temperature is 23 °C), thrust from CFD simulation is found to be 0.22, 0.185, 0.177 mN for $N_2$, CO2 and Argon respectively which increases up to 0.335, 0.282 & 0.268 mN when the propellant temperature is increased up to 500 °C.

### 4.3.3 Specific Impulse:

From the eq. no (27) Specific Impulse calculated to show the effect of specific impulse of three different gas and different heater temperature in Table. 18

| Specific Impulse Isp (s) | | | |
|---|---|---|---|
| **Temperature ( C)** | **Nitrogen** | **Co2** | **Argon** |
| **23** | 65.05 | 54.17 | 51.76 |
| **100** | 71.15 | 59.16 | 54.97 |
| **200** | 77.88 | 65.91 | 61.31 |
| **300** | 85.00 | 71.66 | 66.93 |
| **400** | 90.63 | 77.00 | 72.15 |
| **500** | 97.65 | 81.60 | 78.16 |

Table 18: Specific Impulse of $N_2$, $CO_2$ and Argon across heater temperature

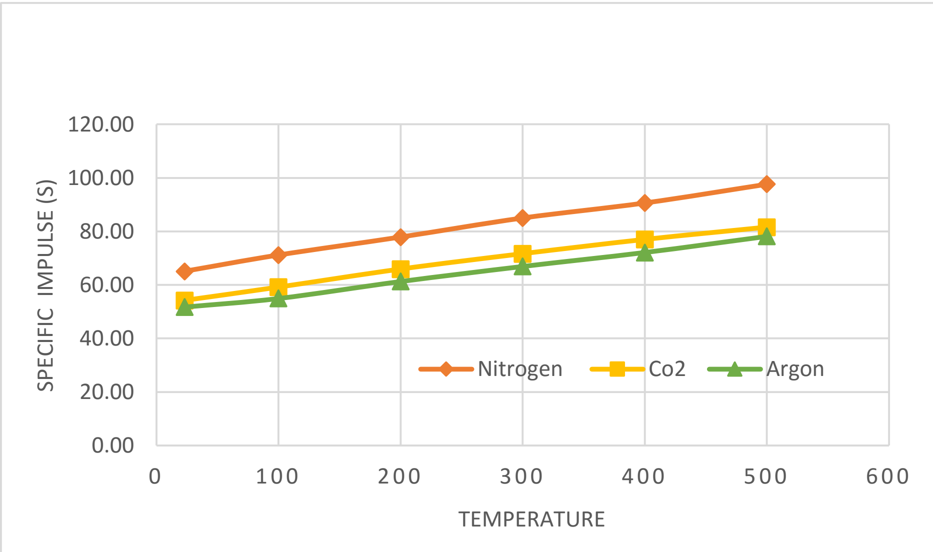


Figure 18: Specific Impulse of $N_2$, $CO_2$ and Argon across heater temperature

Isp of the micro-resistojet also increases from 65.05s, 54.17s, 51.76s to 97.65s, 81.60s &78.16s for $N_2$, $CO_2$ and argon respectively as the heater temperature or the propellant temperature increases from 23 ºC to 500 ºC. It can be seen from the Fig. 22 that there is around 50 % increase in Isp when the heater temperature is increased from 23 ºC to 500 ºC for $CO_2$.$NO_2$, and argon.

### 4.3.4 Subsonic Area:

CFD results for the percentage of nozzle exit area occupied by viscous subsonic layer are shown in Table 19 and its graphical representation shown in Fig.23

| Subsonic Area (%) | | | |
|---|---|---|---|
| **Temperature ( C)** | **NO2** | **CO2** | **Argon** |
| **23** | 24.12 | 23.59 | 28.22 |
| **100** | 25.67 | 24.63 | 33.13 |
| **200** | 28.77 | 25.08 | 33.91 |
| **300** | 29.34 | 25.76 | 34.65 |
| **400** | 30.54 | 25.91 | 35.11 |
| **500** | 29.72 | 26.78 | 35.39 |

Table 19: Subsonic Area of $N_2$, $CO_2$ and Argon across heater temperature

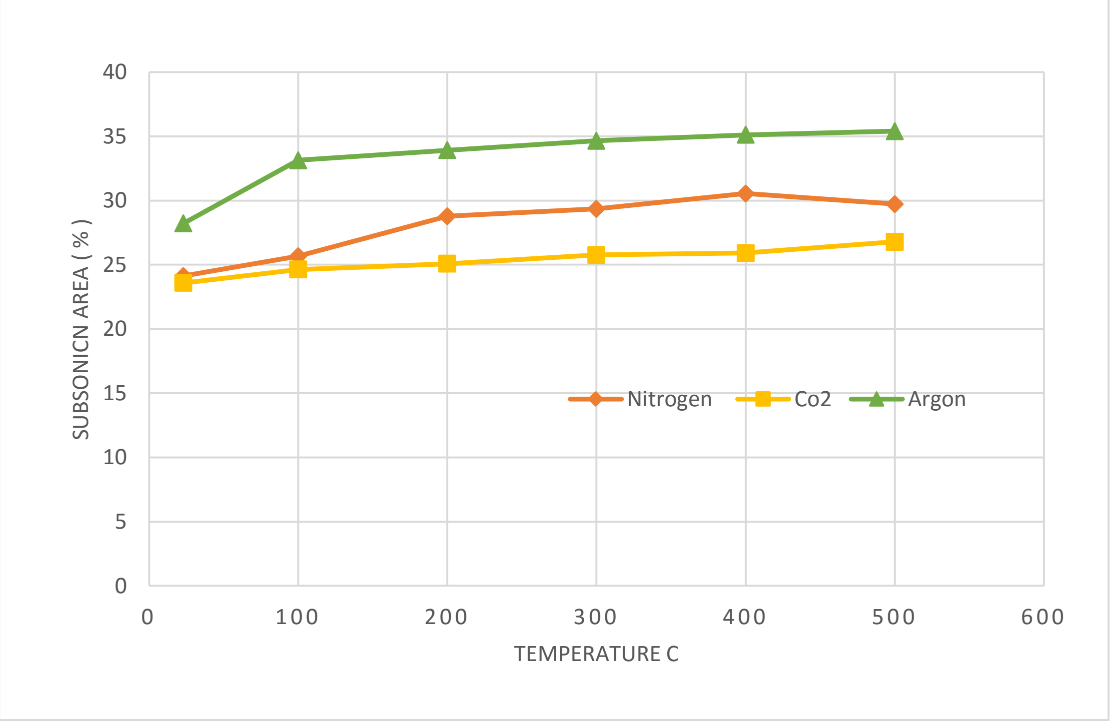


Figure 19: Sub Sonic Area of $N_2$, $CO_2$ and Argon across heater temperature

.From Table 19, and Fig. 23 & 24 It can be seen that by CFD results of nozzle exit cross-section, the viscous subsonic layer slightly increase with heater temperature. So it is predicted that subsonic layer formation didn't effects much in nozzle performance as the heater temperature or the propellant temperature increases from 23 $^oC$ to 500 $^oC$ for the current geometry and simulations.

### 4.3.5 Contours of Mach No:

Maximum Mach No. found at heater temperature of 500 °C. Contours of Mach No. are illustrated in Fig18, 19 & 20 for $N_2$, $CO_2$, and Argon respectively.

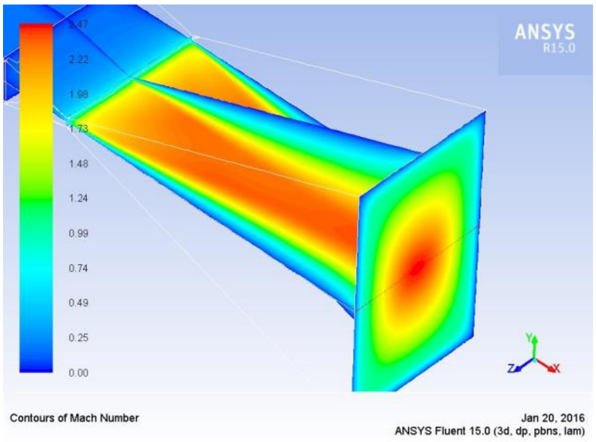


Figure 20: Contour of Mach no. for $N_2$ at 500 °C at

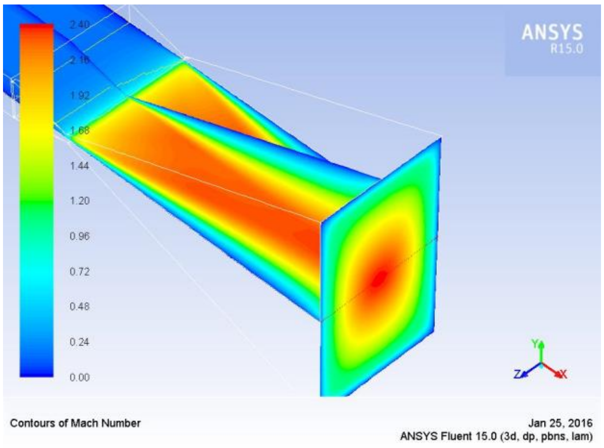


Figure 21: Contour of Mach no. for $CO_2$ 500 C

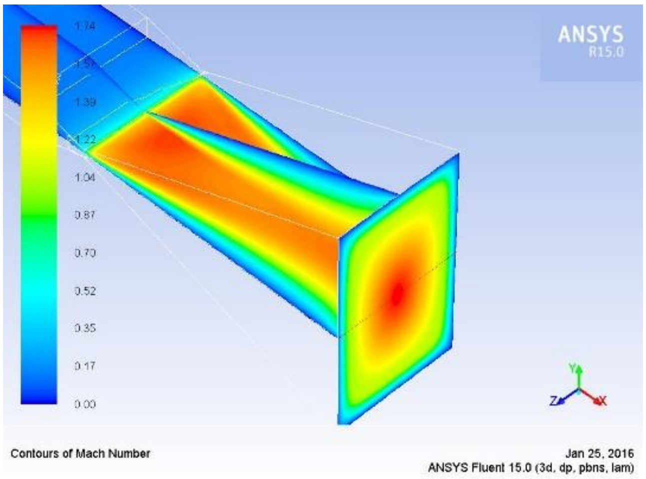


Figure 22: Contours of Mach no. for Argon at 500 C

As shown recent results of nozzle in term of thrust & specific impulse. Similarly Mach No. also highest for $N_2$ then $CO_2$ and then Argon gas at nozzle exit i.e. 2.47, 2.40 & 1.74 respectively. From the above illustration it can be seen that flow is fully developed laminar flow. Predicting maximum velocity at the center of nozzle and sub sonic film around walls. These Subsonic area and maximum velocity comparisons for different gasses and temperature shown in below section 4.3.6 Contours of Subsonic layer and Velocities at Nozzle exit.

### 4.3.6 Contours of Sub Sonic Layer and Velocities at Nozzle Exit.

In Fig 23 the supersonic core region (white area) is removed just to have the clear visibility of the viscous subsonic layer. Fig No.24 shows Contours of (Vx) X-Velocities of gases at nozzle exit. Illustration of velocity contours shows that for same heater temperatures $N_2$ gas highest velocity 998 m/s at 500°C whereas as Argon gas has lowest velocity 777 m/s at 500 °C and CO2 has intermediate velocity 837 m/s at 500°C

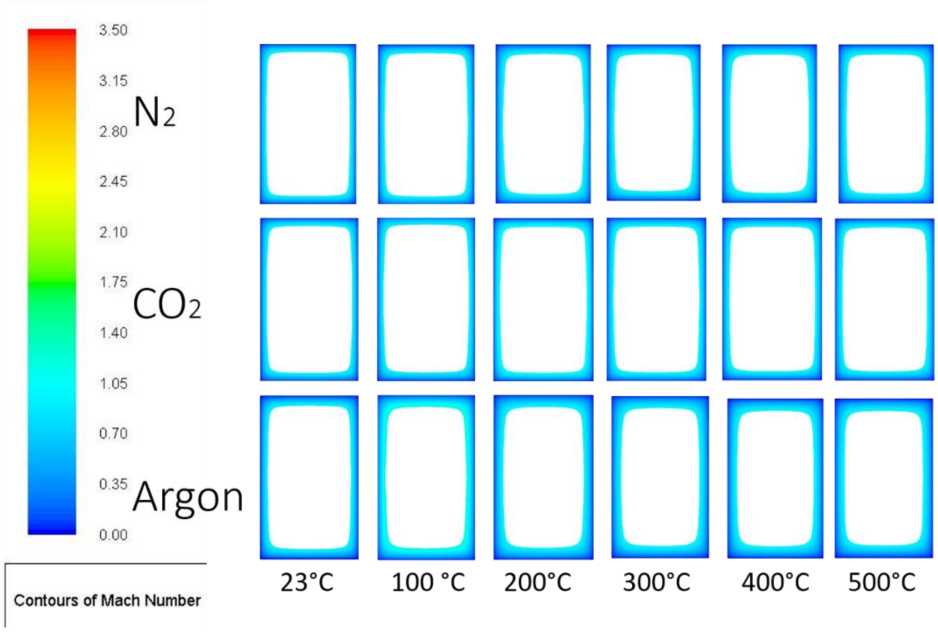


Figure 23: Contours of Sub Sonic Area of $N_2$, $CO_2$ and Argon at the nozzle exit plane across heater temperate

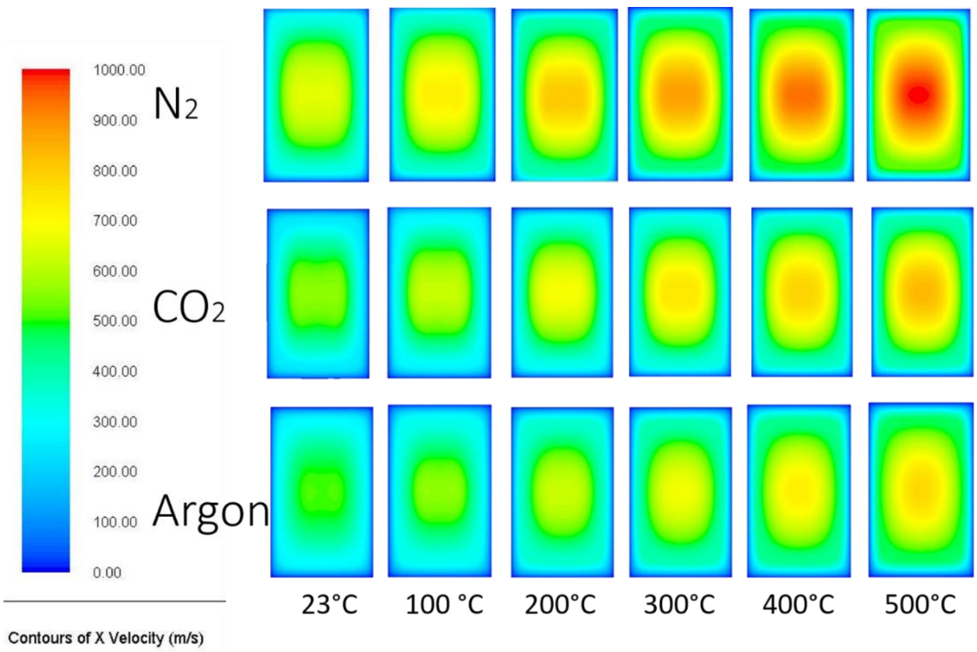


Figure 24: Contours of Velocity ($V_x$) at the Nozzle Exit for $N_2$, $CO_2$, and Argon at the nozzle exit plane across heater temperate

# Chapter 5
# Conclusion

In this report. Numerical investigations of viscous flow through 3-D micro-resistojet thruster are carried out to predict their performance of proposed Micro-Resistojet thruster in the configuration for various working fluids i.e. ($N_2$, CO2, and Argon)

After grid generation study of proposed micro thruster geometry, Numerical CFD Modeling and performance prediction has been done successfully by conducting simulations on a 3-D micro-resistojet thruster with the validation of our numerical CFD method of continuum approach and results from reference experimental data. Continuum approach in supersonic microchannel flows are accounted by Knudsen number which is calculated in our CFD simulation data at the throat region for different heater temperatures and different gasses i.e. $CO_2$, $N_2$ & Argon gases. All calculated values through CFD found to be in the range of continuum flow region i.e. Kn <0.01. Secondly the results parameter validated from TU Delft Experimental data appeared in research paper [28, 29]. Comparing by both experimental parameter with our CFD simulations. It is found that there is maximum error of 24 % and minimum of 16 % that is well understand, as we neglect convection and radiation losses in our simulation and in the research journal [29] reveals itself that the leakage from in their experimental feed system was to be found significant in the order of 20 ~30 %

By these validation, we get the confidence of designing and developing a micro-resistojet thruster has been gained. Then a parametric study conducted to measure the effects of Thrust, Specific Impulse (Isp) and viscous subsonic layer thickness for three different gases (Nitrogen, CO2, and Argon) with different range of propellant temperature on selected design of nozzle. It can be seen that Total Thrust and Specific Impulse (Isp) is increasing linearly with temperature whereas subsonic layer effects on Nozzle exit didn’t decrease widely with increase of temperature hence didn’t effect much on nozzle performance. On comparing these gases over performance parameter, it is predicts that $N_2$ gas gives best fuel performance, secondly $CO_2$ and thirdly Argon gas in terms of thrust and specific impulse (Isp) but if we consider density ratio of fuel. $CO_2$ gas has much better feasibility because it can be taken as a solid in dry ice form by which large amount of fuel could be taken in small volume as compare to $NO_2$ and Argon gas.

The results obtained through this investigations of viscous flow through micro-resistojet thruster in the configuration of different heater temperature with working fluids i.e. ($N_2$, CO2, and Argon). In the same way further studies can be carried out by taking different mass flow rate of gases and evaluate the effect of Total thrust, Specific impulse and subsonic layer formation to further optimized micro thruster design and fuel feasibility

# References


[1] An Introduction to MEMS (Micro-Electromechanical Systems), Loughborough University, PRIME Faraday Partnership, ISBN 1-84402-020-7, January 2002

[2] Reza Ghaffarian, David G. Sutton, Paul Chaffee, Nick Marquez, Ashok K. Sharma, "Thermal and Mechanical Reliability of Five COTS MEMS Accelerometers."

[3] http://www.eeherald.com/section/design-guide/mems_application_introduction.html

[4] Tor- Arne Grönland, Pelle Rangsten, Martin Nese, Martin Lang, "Miniaturization of Components and Systems for Space using MEMS Technology," IAC- 06-B5.5.12

[5] Ernast Vargas Catalan, "Design and Manufacturing of a Rotationally Symmetric Cold Gas Nozzle in Silicon," Master's thesis, Uppsala University, October 2012.

[6] "MEMS Micropropulsion Components for Small Spacecraft," 25th Annual AIAA/USU Conference on Small Satellites.

[7] Herbert R. Shea, "Reliability of MEMS for Space Applications," Proc. of SPIE, Vol. 6111, 61110A, 2006.

[8] Siegfried W. Janson, Henry Helvajian, William W. Hansen and Lt. John Lodmell, "Microthrusters for Nanosatellites," The Second International Conference on Integrated Micro Nanotechnology for Space Applications (MNT99), Pasadena, CA, April 11-15, 1999.

[9] Hiroyuki Koizumi, "Study on Micro Space Propulsion," PhD Thesis, University of Tokyo, Department of Aeronautics and Astronautics, July 2006.

[10] W.F. Louisos, D.L. Hitt, "Assessing the Potential for Condensation in Supersonic Micronozzle Flows," 10th AIAA/ASME Joint Thermophysics and Heat Transfer Conference, 28 June - 1 July 2010, Chicago, Illinois.

[11] Andrew D. Ketsdever, "Micropropulsion manuscript, Rev-," Propulsion Directorate, United States Air Force Research Laboratory, Edwards AFB, CA, USA.

[12] http://www.increase-performance.com/calc-flue-gas-prop.html

[13] http://www.sscspace.com

[14] http://www.en.wikipedia.org/wki/Prisma

[15] http://www.en.wikipedia.org/wiki/ALMASat-1

[16] http://www.almasat.unibo.it/projects/ALMASat-1

[17] S. J. Widdis, Asante, K., Hitt, D.L., Cross, M.W., Varhue, W.J., McDevitt, M.R., "A MEMS-Based Catalytic Microreactor for a $H_2O_2$ Monopropellant Micropropulsion System," IEEE/ASME Transactions on Mechatronics, 2013.

[18] A Monopropellant hydrazine MEMS thruster for Attitude Control of Nanosatellites," Proceeding of the 2010 IEEE Student's Technology Symposium, 3-4 April 2010, IIT kharagpur

[19] Louisos, W. F., and Hitt, D. L., "Viscous Effects on Performance of Two-Dimensional Supersonic Linear Micronozzles," Journal of Spacecraft and Rockets, Vol. 45, No. 4, 2008, pp. 706–715.

[20] Louisos, W. F., and Hitt, D. L., "Influence of Wall Heat Transfer on Supersonic Micronozzle Performance," Journal of Spacecraft and Rockets, Vol. 49, No. 3, May–June 2012.

[21] Hitt, D. L., Zakrzwski, C., and Thomas, M., "MEMS-Based Satellite Micropropulsion via Catalyzed Hydrogen Peroxide Decomposition," Smart Materials and Structures, Vol. 10, No. 6, 2001, pp. 1163–1175.

[22] Louisos, W. F., and Hitt, D. L., "Analysis of Transient Performance of Supersonic Micronozzles," Journal of Spacecraft and Rockets, Vol. 48, No. 2, 2011, pp. 303–311.

[23] Louisos, W. F., and Hitt, D. L., " Heat Transfer and Viscous Effects in 2D and 3D Micro-Nozzles," 37th AIAA Fluid Dynamics Conference, June 25-28, 2007, Miami, FL, AIAA 2007-3987.

[24] J. Kohler , R. Hebden, A. M. Baker, L. Stenmark,, J. L. Moerel, W. Halswijk, "Detailed Design of a Monopropellant Microrocket Engine using MEMS Technology," PowerMEMS 2004, Kyoto, Japan, Nov 28-30, 2004.

[25] R. Hebden, A. M. Baker, L. Stenmark, J. Kohler, J. L. Moerel, W. Halswijk, "Towards the Development of a Monopropellant Microrocket Engine using MEMS Technology," PowerMEMS 2004, Kyoto, Japan, Nov 28-30, 2004.

[26] http://www.waynesthisandthat.com/ep2.htm

[27] Tittu Varghese Mathew, B. T. C. Zanderbergen, Marko Mihailovic, J. F. Creemer, P. M. Sarro, “A Silicon-Based MEMS Resistojet for Propelling Cubesats”, 62nd IAC, Cape Town, SA, 2011.

[28] M. Mihailovic, J. F. Creemer, B.T.C. Zandbergen and P.M. Sarro, “MEMS Silicon-Based Resistojet Micro-Thruster for Attitude Control of Nanosatellites,” Proceedings of the Transducers '11 conference (pp. 262-265), 2011, Beijing, China.

[29] Ir B.T.C Zandbergen , T. V. Mathew Design of MEM Micro Resistojet Research Journal of DIMES Delft Institute of Microelectronics and subsonic Technology , published in 22 Jun 2011

[30] Ketsdever, A.D., “Facility Effects on Performance Measurements of Micropropulsion Systems that Utilize Gas Expansion,” Journal of Propulsion and Power, Vol. 18, No. 4, pp.797–804, 2002.

[31] Lempert, W.R., Boehm, M., Jiang, N., Gimelshein, S. and Levin, D., “Comparison of Molecular Tagging Velocimetry Data and Direct Simulation Monte Carlo Simulations in Supersonic Micro Jet Flows,” Experiments in Fluids, Vol. 34, No. 3, pp.403–411, 2003.

[32] Ketsdever, A.D., Clabough, M.T., Gimelshein, S.F. and Alexeenko, A.A., “Experimental and Numerical Determination of Micropropulsion Device Efficiencies at Low Reynolds Numbers,” AIAA Journal, Vol. 43, No. 3, pp.633–641.

[33] Louisos, W. F., Alexeenko, A. A., Hitt D. L., and Zilic, A., “Design Considerations for Supersonic Micronozzles,” International Journal of Manufacturing Research, Vol. 3, No. 1, 2008, pp. 80–113.

[34] https://www.grc.nasa.gov

[35] https://www.sharcnet.ca/Software/Fluent6/html/ug/node1021.htm

[36] Stanley P. Grisnik and Tamara A. “Experimental Study of Low Reynolds Number Nozzles” (USA-Tfl-89858) EXPE3lflENTAL STUDY OP LOY BEYBCLDS EUEIeEB LCZZLES (NASA) 13 p CSCL 21H 387-26363 Unclas 63/20 45424